Journal Pre-proofs

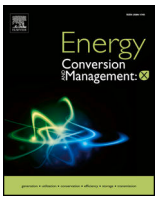


# Investigation of the operating characteristics of a free-piston closed-cycle Joule engine generator with helium as working fluid

Benlei Wang, Shunmin Zhu, Ugochukwu Ngwaka, Boru Jia, Kumar Vijayalakshmi Shivaprasad, Yaodong Wang, Andrew Smallbone, Anthony Paul Roskilly, Ercang Luo

PII: S2590-1745(25)00041-8
DOI: https://doi.org/10.1016/j.ecmx.2025.100909
Reference: ECMX 100909

To appear in: *Energy Conversion and Management: X*

Received Date: 13 August 2024
Revised Date: 6 January 2025
Accepted Date: 1 February 2025

Please cite this article as: B. Wang, S. Zhu, U. Ngwaka, B. Jia, K. Vijayalakshmi Shivaprasad, Y. Wang, A. Smallbone, A. Paul Roskilly, E. Luo, Investigation of the operating characteristics of a free-piston closed-cycle Joule engine generator with helium as working fluid, *Energy Conversion and Management: X* (2025), doi: https://doi.org/10.1016/j.ecmx.2025.100909

# Investigation of the operating characteristics of a free-piston closed-cycle Joule engine generator with helium as working fluid

Benlei Wang[a,b], Shunmin Zhu[c,*], Ugochukwu Ngwaka[c], Boru Jia[d], Kumar Vijayalakshmi Shivaprasad[c], Yaodong Wang[c], Andrew Smallbone[c], Anthony Paul Roskilly[c], Ercang Luo[a,b,*]

[a]*Key Laboratory of Cryogenic Science and Technology, Technical Institute of Physics and Chemistry, Chinese Academy of Sciences, Beijing 100190, China*

[b]*University of Chinese Academy of Sciences, Beijing 100049, China*

[c]*Department of Engineering, Durham University, Durham, DH1 3LE, UK*

[d]*School of Mechanical Engineering, Beijing Institute of Technology, Beijing 100081, China*

**Corresponding authors: shunmin.zhu@durham.ac.uk (S. Zhu), ecluo@mail.ipc.ac.cn (E. Luo)*

## Abstract:

As an emerging micro- or small-scale energy conversion technology, linear Joule engine generators (LJEGs) combine the advantages of external combustion engines and linear generators, feature the advantages of high thermal-to-electrical efficiency, multi-fuel potential, good operational flexibility, a simple and compact mechanical structure, and low frictional loss. Earlier research on LJEGs mainly focused on open-cycle systems, while closed-cycle LJEGs, which are the subject of this work, have some unique characteristics in comparison with open-cycle ones. Unfortunately, the operating features of closed-cycle LJEGs are still not well comprehended. To fill this gap, in this paper, the operating characteristics of a closed-cycle LJEG with helium as working fluid are investigated based on a validated numerical model. The dynamic characteristics and output performance of the system were investigated at different system pressures and compared with an open-cycle LJEG with air as working fluid. The outcomes reveal that the closed-cycle LJEG has a smaller piston stroke and higher output efficiency. Furthermore, the effect of key parameters such as valve timing, electrical resistance coefficient, and cylinder diameters on system performance is investigated. This study offers in-depth insights into the operation characteristics of the closed-cycle LJEG, which contributes to the design of similar systems.

## Keywords:

energy conversion; free-piston; linear Joule engine generator; closed Brayton cycle; helium

**Nomenclature**

***Symbols***

| | |
|---|---|
| $A$ | cross-section area ($m^2$) |
| $C$ | heat capacity rate |
| $C_e$ | load constant of the linear generator ($N/(m \cdot s^{-1})$) |
| $C_k$ | dynamic friction coefficient |
| $C_p$ | specific heat capacity at constant pressure ($J/(kg \cdot K)$) |
| $C_s$ | static friction coefficient |
| $C_v$ | specific heat capacity at constant volume ($J/(kg \cdot K)$) |
| $D$ | effective diameter (m) |
| $F$ | force (N) |
| $f$ | operating frequency (Hz) |
| $F_e$ | generated electromagnetic resistance force (N) |
| $F_f$ | friction force (N) |
| $v$ | velocity of the mover (m/s) |
| $v_p$ | the average speed of the piston (m/s) |
| $W_i$ | work done by the linear compressor piston (J) |
| $x$ | piston displacement (m) |
| $\alpha$ | electrical resistance coefficient |
| $\gamma$ | specific heat ratio |
| $\varepsilon$ | effectiveness of the heater |
| $\rho$ | gas density ($kg/m^3$) |
| $\Phi$ | magnetic flux (Wb) |

***Subscripts***

| | |
|---|---|
| c | cold-fluid |
| com | compressor |
| com.l | left side of the compressor cylinder |
| com | right side of the compressor |

| | | | |
|---|---|---|---|
| | | .r | cylinder |
| $h$ | specific enthalpy of the working fluid (J/kg) | exp | expander |
| $i$ | current (A) | exp.l | left side side of the expander cylinder |
| $K_A$ | electromagnetic force constant | exp.r | right side of the expander cylinder |
| $K_v$ | the back EMF constant of the linear generator | h | hot-fluid |
| $m$ | mass (kg) | max | maximum |
| $P$ | gas pressure (Pa) | min | minimum |
| $P_{com.in}$ | compressor intake pressure (Pa) | surf | the surface area |
| $P_{com.out}$ | exhaust pressure of the compressor (Pa) | w | the cylinder wall surface |
| $Q$ | heat received by the system from the surroundings (J) | | |
| $R_g$ | gas constant (J/(kg·K)) | ***Abbreviations*** | |
| $R_L$ | external load resistance (Ω) | | |
| $R_S$ | internal resistance of the linear generator (Ω) | CHP | combined heat and power |
| $S$ | piston stroke (m) | EMF | electromotive force |
| $T$ | temperature (K) | LDC | left dead center |

| | | | |
|---|---|---|---|
| $t$ | time (s) | LJEG | linear Joule engine generator |
| $U$ | internal energy of the gas (J) | RDC | right dead center |
| $V$ | volume of the cylinder ($m^3$) | | |

## 1. Introduction

Nowadays, energy shortages and climate crises are becoming more and more serious worldwide. Developing small- or micro-scale distributed energy systems is considered a viable option to improve energy utilization efficiency [1, 2]. For conventional, centralized energy systems, like gas turbines [3] (operating on Brayton cycle) and steam power plants [4] (Rankine cycle), miniaturization while maintaining high efficiency poses a significant challenge. For example, when a gas turbine's power capacity is reduced to a few kilowatts, its efficiency drops sharply. Typically, compact rotodynamic equipment is plagued by suboptimal performance, primarily attributed to challenges in sealing mechanisms and the detrimental effects of frictional losses [5, 6]. Meanwhile, the commonly used internal combustion engines, like gasoline and diesel engines, are specifically engineered to exclusively consume fossil fuels, thereby lacking the capability to harness external heat sources in their operation [7]. Although Stirling engines with external combustion can utilize various heat sources [8, 9], their low efficiency at partial load and high cost on a small scale hinder their wide application [10]. In this context, there is a need to propose and develop new prime mover technologies capable of delivering high-efficiency power generation on a modest scale—ranging from 1 kWe to 100 kWe—and that are adaptable to an array of eco-friendly heat sources, including but not limited to waste heat, solar energy, nuclear power, and geothermal resources, as well as conventional fossil fuels.

Linear Joule engine generators (LJEGs) promise to be an attractive solution to this challenge. A linear generator plus a linear Joule engine makes up a typical LJEG. The linear Joule engine is an external combustion engine. It utilizes the synergy between the expander and compressor to achieve a linear reciprocating motion of the two connected pistons (i.e., the expander piston and compressor piston), thus producing power output for external use (e.g., driving a linear generator to generate electricity). Its nature of external heat supply allows it to draw energy from a spectrum of eco-friendly sources, encompassing solar power, biomass, and nuclear energy, in addition to traditional fossil fuels. The linear generator can produce electrical energy through the reciprocating, linear motion of a coil or magnets in a magnetic field or a stationary coil [11-13]. LJEGs combine the respective advantages of linear generators and linear Joule engines, with high thermal-to-electric conversion efficiency, extensive fuel adaptability, and great operational flexibility [14]. These characteristics make it a promising candidate in the fields of small- and micro-scale cogeneration systems, electric vehicle range extenders, solar power generations, and mobile power supplies.

The theoretical thermodynamic cycle of LJEGs follows the Brayton cycle, which can take the form of open, semi-closed, and closed cycles [15]. Open-cycle and semi-closed-cycle LJEGs achieve heat input through the combustion of fuel and air in external-combustion chambers. In contrast, closed-cycle LJEGs complete the entire thermodynamic cycle in a closed loop [16]. The working fluid undergoes heating by an external heater and cooling by a cooler unit, and the expander exhausts are recirculated rather than expelled. Unlike open-cycle and semi-closed-cycle LJEGs, closed-cycle systems exhibit only heat exchange from the external heater to the working fluid, with no mass exchange.

The original concept of LJEG was proposed by Mikalsen and Roskilly in 2012 [5]. In reference [5], the effects of combustion temperature, cylinder size and other parameters on the engine performance of the system were preliminarily investigated, which guided the determination of the optimal design configuration. Later, numerous works that aimed at improving the technology readiness level (TRL) of the LJEG, especially of the open-cycle LJEG, have been presented, mainly concentrating on system modelling [17-23], prototype development [24, 25], and linear generator (applied to LJEGs) development [26-28].

Firstly, in 2017, a numerical model that integrates a Joule engine with a permanent magnet linear generator was proposed [17]. This model offers enhanced simulation accuracy over the conventional approach, which employs a damper to emulate a linear alternator. Later, Jia et al. [18] developed a zero-dimensional computational model designed to assess the kinetic and thermal properties within open cycle LJEG systems. The model illustrates the basic operating characteristics of the LJEG. Subsequently, the research team studied the kinetic and thermal properties of the system under different working conditions and identified key parameters that affect system [19]. The linear Joule engine eliminates the crankshaft mechanism in a conventional Joule engine, and its total friction loss is reduced compared with that of a crankshaft Joule engine [20-22]. To study the friction process of the LJEG in detail, Ngwaka et al. developed a friction model for dynamic LJEG simulation [23]. The research found that, aside from the surface traits, the system pressure and the movements of the piston are the predominant influences on the friction within an LJEG. The study also concluded that a large resistance could lead to less friction and improve the efficiency of the system.

The above-mentioned numerical works pave the way for the following prototype development of LJEG. Wu and Roskilly designed an LJEG prototype and optimized its geometric parameters [24]. This study highlights the potential of LJEG for high efficiency at micro-scales and its suitability for renewable energy applications. Later, they developed a prototype using the optimised design parameters of previous studies [25].

As a key component in an LJEG, the development of linear generators for LJEG applications has received considerable attention. Jalal et al. [26] designed a tubular moving magnet linear alternator using 2D finite-element modelling. Later, they studied the effect of the influence exerted by distinct energy conversion methodologies on linear generator performance metrics when driven by an LJEG [27]. They also investigated the influence of the alternator’s inductive properties and the overall electromagnetic forces exerted on it, examining how these factors contribute to the resultant force experienced by the system. [28].

The aforementioned studies have revealed the operating characteristics of open-cycle LJEGs with air as a working fluid. To explore the operational effectiveness of the LJEG with alternative working fluids, Ngwaka et al. [29] proposed an LJEG based on semi-closed cycle. Leveraging the physical characteristics of argon and hydrogen and oxygen combustion efficiency, the system's efficiency is more than 60% compared to its open-cycle counterpart.

Compared to open-cycle and semi-closed-cycle engines, closed-cycle linear Joule engines offer several advantages: (i) In a typical closed-cycle linear Joule engine, the working

fluid is isolated from the external environment. This isolation allows for using gases like helium, argon, nitrogen, or gas mixtures, enhancing thermodynamic performance. (ii) The choice of heat source and heat sink is flexible in closed-cycle LJEGs. For instance, heat sources can be derived from fossil or biomass fuels, with complete combustion under optimal conditions. Alternatively, LJEGs can harness clean energy sources like concentrated solar or nuclear energy. (iii) Unlike other engines, the closed-cycle engine does not require air or oxygen consumption, rendering it suitable for deep-sea or space applications. Considering these advantages, closed-cycle LJEGs exhibit excellent environmental adaptability and promising application prospects. Hence, further exploration of their operating characteristics is imperative. The only work at the time of writing concentrating on closed-cycle LJEGs was performed by Li et al. [30]. They investigated the impact of different working fluids on a closed-cycle LJEG's performance and revealed the relationship between system frequency, system pressure and engine efficiency. The system's power output, thermal efficiency, peak pressure, and other characteristics are significantly impacted by the working medium's specific heat ratio.

Choosing the appropriate working fluid in a closed-cycle engine is pivotal, as it can influence the system's configuration, size and performance. According to previous research on closed-cycle LJEGs and other closed-cycle engines (such as closed-cycle gas turbines, Stirling engines, and closed-cycle diesel engines), helium is considered an ideal working medium, favoured for its array of beneficial properties. These include a high specific heat at constant pressure, high heat transfer coefficient, low-pressure losses, and good compressibility [31]. Therefore, a thorough investigation into the operational characteristics of a closed-cycle LJEG utilizing helium as the working fluid is essential for its design and continued advancement. While previous studies have explored closed-cycle LJEGs employing different working fluids to some extent [30], a comprehensive understanding of their operational dynamics remains incomplete, particularly in systems employing helium as the primary working fluid. Therefore, the current work aims to fill this gap through a comparative analysis between closed-cycle and open-cycle LJEGs operating under identical conditions and further explore the influence of pivotal system parameters on overall performance. This analysis is poised to provide invaluable insights to inform the design of future prototypes.

Following is the arrangement of the paper: First, the development of the LJEG is reviewed. Next, the configuration and working principle of the closed-cycle LJEG system considered in this study are briefly introduced. Following this, a detailed zero-dimensional model, developed and validated using results from previous studies, is presented. Based on the validated model, an exploration of the fundamental operational traits of the closed-cycle LJEG utilizing helium as the working medium is conducted. In extension, the effects of key parameters on the system performance is examined and conclusions are drawn.

## 2. System configuration and operating principles

The configuration of the closed-cycle LJEG considered in this work is shown in Figure 1. It consists of five primary components: a compressor, an expander, an external heater, a cooler and a linear generator. Both the expander and compressor pistons employ a double-acting configuration, contributing to the system's enhanced compactness. The respective cylinders of the compressor and expander are divided into two relatively independent chambers. The piston rods of these two pistons are linked to the linear generator's mover, which is centrally positioned between the expander and the compressor. The external heater and cooler are located between the compressor and the expander, each of which are connected to the expander and compressor by pipes.

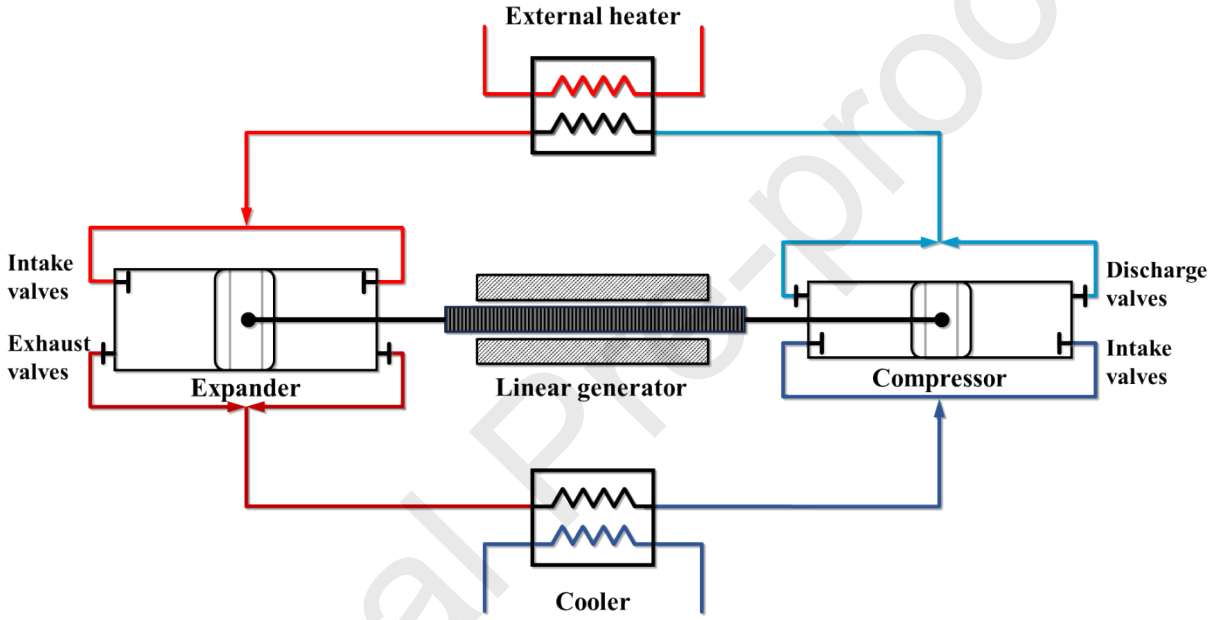


**Figure 1.** Schematic of the LJEG considered in this work.

During operation, the working fluid enters the compressor through the intake valves. After compression, the working fluid is discharged through the discharge valve and enters directly into the heater for heating. Subsequently, the intake valve of the expander is opened, and the working fluid enters the expander and drives the expander piston to move in a straight line. The expanded gas then flows into the cooler for cooling. Due to the rigid connection between the pistons and the translator, the linear motion of the expander piston causes a motion in the generator translator, resulting in the cutting of the magnetic field lines and the generation of electricity. Concurrently, the compressor piston is also driven by the expander piston to compress the working fluid in the other-side cylinder to prepare for the next cycle.

The ideal thermodynamic cycle for a linear Joule engine, comprising four key processes: isentropic compression within the compressor, isobaric heat addition [32], isentropic expansion within the expander, and isobaric heat rejection, illustrated in Figure 2.

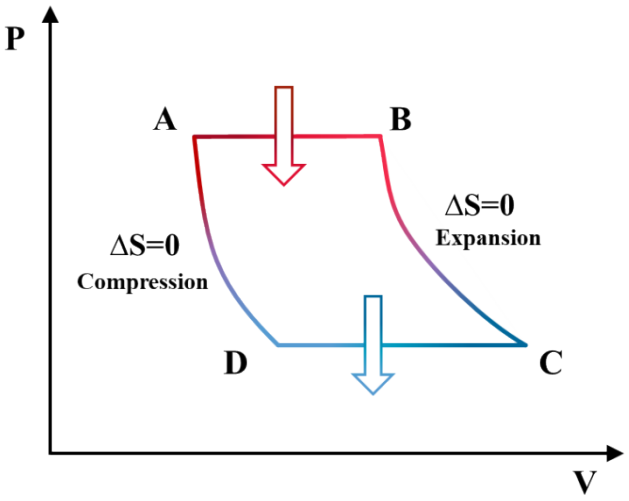


**Figure 2.** *P-V* diagram for the ideal Joule cycle.

## 3. Model description and validation

### 3.1 Model structure

Based on the LJEG's working principle, the system's energy input comes from the external heater. As the gas drives the expander to do work, its final output is electrical energy. Different numerical sub-models characterize the LJEG's dynamic and thermodynamic characteristics, including piston motion states, pressure variations within the expander and compressor cylinders, as well as the system's output power.

#### 3.1.1 Piston dynamics sub-model

Unlike a crankshaft Joule-cycle engine [21], the two pistons of the LJEG are not limited by a crankshaft mechanism, and the forces acting on the mover (including the connecting rod, two pistons, and the translator of the linear generator) determine its motion state. As shown in Figure 3, the movement of the mover is affected by the gas forces exerted by the gas, the electromagnetic resistance and the system's friction force. Following the Newton's second law, we have [33]:

$$\overrightarrow{F_{\mathrm{exp}}} + \overrightarrow{F_{\mathrm{com}}} + \overrightarrow{F_{\mathrm{e}}} + \overrightarrow{F_{\mathrm{f}}} = m\vec{a} (1)$$

$$\overrightarrow{F_{\mathrm{exp}}} = \overrightarrow{F_{\mathrm{exp.l}}} + \overrightarrow{F_{\mathrm{exp.r}}} (2)$$

$$\overrightarrow{F_{\mathrm{com}}} = \overrightarrow{F_{\mathrm{com.l}}} + \overrightarrow{F_{\mathrm{com.r}}} (3)$$

where $\overrightarrow{F_{\mathrm{exp}}}$ and $\overrightarrow{F_{\mathrm{com}}}$ are the gas force acting on the expander piston and the compressor piston, respectively. Subscript $l$ and $r$ denote the left and right chambers, respectively. $\overrightarrow{F_{\mathrm{e}}}$ denotes the electromagnetic resistance force, and $\overrightarrow{F_{\mathrm{f}}}$ indicates the frictional force.

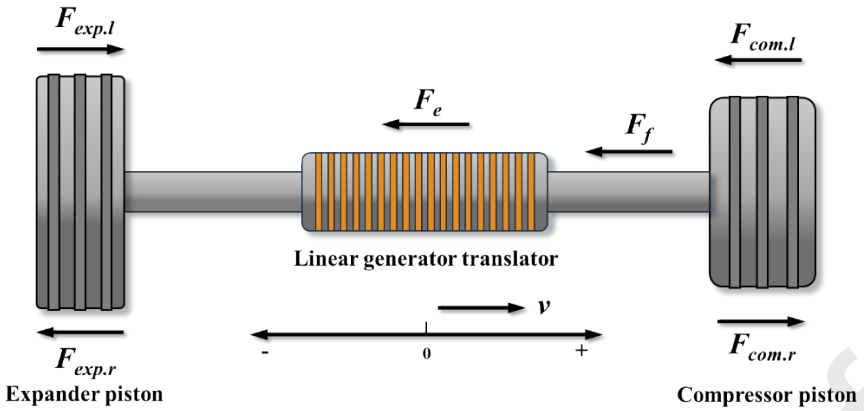


**Figure 3.** Diagram of the force acting on the mover.

In the four compressor and expander chambers, the force acting on the respective piston by the working fluid is determined by multiplying the gas pressure by the piston's effective area:

$$\overrightarrow{F_{\mathrm{exp.l}}} = P_{\mathrm{exp.\,1}} \times \mathrm{A}_{\mathrm{exp}} (4)$$

$$\overrightarrow{F_{\mathrm{exp.r}}} = P_{\mathrm{exp.\,r}} \times \mathrm{A}_{\mathrm{exp}} (5)$$

$$\overrightarrow{F_{\mathrm{com.l}}} = P_{\mathrm{com.\,1}} \times \mathrm{A}_{\mathrm{com}} (6)$$

$$\overrightarrow{F_{\mathrm{com.r}}} = P_{\mathrm{com.r}} \times \mathrm{A}_{\mathrm{com}} (7)$$

where $P_{\mathrm{exp}}$ is the gas pressure at the expander and $P_{\mathrm{com}}$ denotes the gas pressure at the compressor; $A_{\mathrm{exp}}$ and $A_{\mathrm{com}}$ are the cross-section area of the expander piston and the cross-section area of the compressor piston, respectively.

### 3.1.2 Linear compressor sub-model

The gas in the cylinders affects the motion of the mover, and the motion of the mover, in turn, influences the state of the working fluid. A balance is achieved when the system is in normal working condition. To facilitate the coupling of the working fluid's thermodynamic model with the comprehensive system model, the following suppositions are established:

(1) The gas in the compressor and expander cylinders is considered an ideal gas. In the compression or expansion process, its specific heat capacity is regarded as a constant and does not change with temperature.

(2) The seals between each valve and its seat and between the piston ring and the cylinder liner are good, without gas leakage.

(3) The intake and exhaust processes are considered ideal. Upon opening the valve, the pressure is the same as the intake/exhaust pressure. The energy loss caused by gas flow is ignored, and the influence of pressure drop is not considered.

The linear compressor is a vital component of the LJEG system. It is where the working fluid's isothermal compression process occurs, providing high-pressure gas to the heater. The linear compressor comprises a double-acting piston, two intake and two discharge valves, and a cylinder. Due to the existence of the double-acting piston, the cylinder is divided into two chambers, each with its own intake and exhaust valves.

The governing thermodynamic equation for the gas within the cylinder is presented as:

$$dQ = dU + dW_{\mathrm{i}} (8)$$

where $Q$ is the heat received by the system from the surroundings, $U$ indicates the internal energy of the working fluid, and $W_{\mathrm{i}}$ indicates the work done by the linear compressor piston.

For the ideal gas, the internal energy is only a function of temperature, and it is given as：

$$dU = m \cdot C_v \cdot (9)$$

where $m$ represents the mass of the working fluid inside the cylinder, $C_v$ represents the specific heat capacity at constant volume, $T$ is the temperature of the gas in the cylinder.

The work done by the working fluid pushing the piston can be expressed as:

$$\delta W_{\mathrm{i}} = P_{\mathrm{com}} \cdot dV_{\mathrm{com}} (10)$$

where $P_{\mathrm{com}}$ indicates the pressure of the working fluid in the compressor cylinder, $V_{\mathrm{com}}$ denotes the volume on one side of the compressor. From Equations (8)-(10), we can deduce that:

$$\delta Q = mC_v dT + P_{\mathrm{com}} dV_{\mathrm{com}} (11)$$

Taking the derivative of the two sides of the equation with respect to time:

$$\frac{\delta Q}{dt} = m\frac{C_v dT}{dt} + P_{\mathrm{com}}\frac{dV_{\mathrm{com}}}{dt} (12)$$

According to the ideal gas state equation:

$$P_{\mathrm{com}} dV_{\mathrm{com}} + V_{\mathrm{com}} dP_{\mathrm{com}} = mR_{\mathrm{g}} (13)$$

As derived from Equations (12) and (13):

$$\frac{\delta Q}{dt} = P_{\mathrm{com}}\frac{C_v + R_{\mathrm{g}}}{R_{\mathrm{g}}} \cdot \frac{dV_{\mathrm{com}}}{dt} + \frac{C_v V_{\mathrm{com}}}{R_{\mathrm{g}}}\frac{dP_{\mathrm{com}}}{dt} (14)$$

Utilizing the Mayer relation [32],

$$R_{\mathrm{g}} = C_{\mathrm{p}} - C_{\mathrm{v}} (15)$$

where $C_p$ is the specific heat capacity at constant pressure, and $R_g$ is the gas constant. The following equation can be derived from Equations (14)-(15) and can be used to calculate the compression process of the compressor.

$$\frac{dP_{com}}{dt} = \frac{\gamma - 1}{V_{com}}\frac{\delta Q}{dt} - \frac{\gamma P_{com}}{V_{com}}\frac{dV_{com}}{dt} \quad (16)$$

where $\gamma$ stands for the specific heat ratio. Employing the Hohenberg model [34] to characterize the heat transfer:

$$\delta Q = 130V^{-0.06}\left(\frac{P(t)}{10^5}\right)^{0.8} T^{-0.4}\left(v_p + 1.4\right)^{0.8} \cdot A_{com.surf}(T - T_w) \quad (17)$$

where $\delta Q$ is the heat flow rate, $V$ is the instantaneous cylinder volume, $v_p$ is the average speed of the piston, $A_{com,surf}$ represents the surface area of the gas in contact with the cylinder, and $T_w$ is the average temperature at the cylinder wall surface.

Combined with the previous assumptions, the gas pressure in the cylinder's one chamber can be represented as:

$$P_{com2} = \begin{cases} P_{com.out}; & P_{com2} \geq P_{com.out} \\ P_{com1}\left(V_{com1}^{\gamma}/V_{com2}^{\gamma}\right); & P_{com.in} < P_{com2} < P_{com.out} \\ P_{com.in}; & P_{com2} \leq P_{com.in} \end{cases} \quad (18)$$

where $P_{com.out}$ is the exhaust pressure of the compressor, which is the same as the intake pressure of the expander; $P_{com.in}$ is the compressor intake pressure. During the steady operation of the compressor, if we neglect gas leakage, the gas mass flow rate through the valves can be expressed as follows [35]:

$$\dot{m} = \frac{1}{2}\pi x_{com}\rho_{com}D_{com}^2 \quad (19)$$

where $x_{com}$ is the piston displacement within a compression stroke, $\rho_{com}$ is the gas density in the compressor, and $D_{com}$ is the effective diameter of the compressor piston.

### 3.1.3 Linear expander sub-model

The linear expander is a primary component in the system, which outputs mechanical work to the linear generator. Similar to the linear compressor, the linear expander is mainly composed of a double-acting piston, two electromagnetic intake valves, two electromagnetic exhaust valves, and a cylinder. The gas heated by the external heater enters the cylinder of the expander and pushes the expander piston back and forth, thereby completing the isothermal expansion process.

Within the expander's cylinder, the primary thermodynamic events encompass piston-induced gas compression and expansion, heat exchange between the fluid and the walls, and intake and exhaust processes. All of these thermal processes are similar to those of the linear compressor, except that during the expansion process, the gas continuously enters the expansion

chamber, which causes the energy change within the control volume. Therefore, the pressure of the cylinder on either side of the expander can be expressed as [18]:

$$\frac{dP_{\text{exp}}}{dt} = \frac{\gamma - 1}{V_{\text{exp}}}\frac{dQ}{dt} - \frac{\gamma P_{\text{exp}}}{V_{\text{exp}}}\frac{dV_{\text{exp}}}{dt} + \frac{\gamma - 1}{V_{\text{exp}}}\sum_{i}\dot{m}_{\text{exp.i}}\,h_{\text{exp.i}} \quad (20)$$

where $P_{\text{exp}}$ is the gas pressure within either side of the expander cylinder, $V_{\text{exp}}$ is the instantaneous volume of the expander cylinder on one side, $\dot{m}_{\text{exp.i}}$ is the mass flow rate entering or leaving the cylinder, and $h_{\text{exp.i}}$ is the specific enthalpy of the working fluid. The linear expander's heat transfer model and mass flow rate are the same as those of the linear compressor and will not be reiterated herein.

### 3.1.4 Linear generator sub-model

During operation, the linear generator translator moves reciprocally under the push of the expander piston, cutting the magnetic induction lines, and generating induced current in the generator's stator coil accordingly. Figure 4 presents the equivalent circuit diagram for the linear generator.

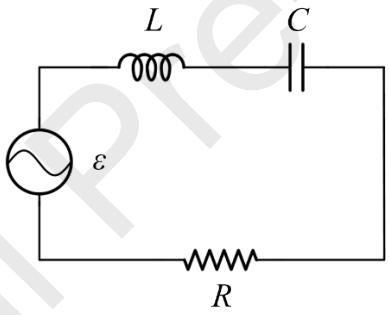


**Figure 4.** Equivalent circuit diagram of the linear generator.

The electromotive force (EMF) $\varepsilon(t)$ can be formulated as follows:

$$\varepsilon(t) = -N\frac{d\Phi}{dt} = -K_{\text{v}}\frac{dx}{dt} = -K_{\text{v}} \cdot v \quad (21)$$

where $\Phi$ is the magnetic flux, and $K_{\text{v}}$ is the back EMF constant of the linear generator, which can be found in the linear generator specifications. $x$ is the displacement of the generator translator, $v$ is the velocity of the generator translator, which is equal to the motion velocity of the two pistons.

The induced current in the generator coil is determined by the EMF and the circuit load. Assuming the load circuit is purely resistive, the induced current can be expressed as:

$$i(t) = \frac{\varepsilon(t)}{R_{\text{s}} + R_{\text{L}}} \quad (22)$$

where $i$ denotes the current, $R_S$ denotes the internal resistance of the linear generator, and $R_L$ represents the external load resistance. The foregoing two equations lead to the following relationship:

$$i(t) = -\frac{K_v}{R_S + R_L} \cdot (23)$$

When a linear motor operates in a generator mode, the generated electromagnetic resistance force can be represented as [35]:

$$F_e = -C_e \cdot (24)$$

where $C_e$ is the load constant of the linear generator. Neglecting inductive loads, its calculation formula can be expressed as [36]:

$$C_e = K_A \cdot K_V \cdot \frac{1}{R_S + R_L} (25)$$

where $K_A$ is the electromagnetic force constant. The values of $K_A$, $K_v$ and $R_s$ are all determined based on the linear generator's specifications.

### 3.1.5 Frictional force sub-model

Owing to the absence of the crankshaft and the crank-connecting rod mechanism, the friction loss of the LJEG system is significantly reduced in contrast to conventional internal combustion engines. The frictional force is articulated by the following expression [37]:

$$F_f = -(C_k \cdot |v| + C_s) \cdot (26)$$

where $C_k$ is the dynamic friction coefficient; $C_s$ represents the static friction coefficient, constituting its invariant component within the frictional force.

### 3.1.6 Heater and cooler sub-models

The process of heat absorption and heat rejection of the working fluid are essential parts of the engine's energy conversion. Given the external heating characteristics of the closed-cycle LJEG, the heating and cooling processes are realized through heat exchangers. The heat absorbed by the working fluid can be depicted based on the first law of thermodynamics:

$$Q = \dot{m}(h_B - h_A) = \dot{m}(c_{pB}T_B - c_{pA}T_A) (27)$$

where $\dot{m}$ represents the mass flow rate of the working fluid, $h_B$ indicates the specific enthalpy at the outlet of the heater, and $h_A$ indicates the specific enthalpy at the inlet of the heater. For the modelling approach of the heater, a method that assumes an appropriate value for their effectiveness is adopted [38]. Generally, the effectiveness of the heater can be expressed as:

$$\varepsilon = \frac{\dot{Q}}{C_{min}(T_{h,i} - T_{c,i})} (28)$$

where $\varepsilon$ indicates the effectiveness of the heater, $\dot{Q}$ indicates the heat transfer rate, $C_{\min}$ denotes the minimum of $C_h$ (hot-fluid heat capacity rate) and $C_c$ (cold-fluid heat capacity rate), $T_{h,i}$ and $T_{c,i}$ represent the temperatures of the hot and cold fluids entering the heater. For this system, the heating effectiveness can be expressed as:

$$\varepsilon = \frac{T_{h,i} - T_{h,o}}{T_{h,i} - T_{l,i}} (29)$$

According to previous studies on closed-cycle gas turbine heaters, the effectiveness value can reach more than 80% [39]. To ensure the study's objectivity and reliability, the heater's effectiveness is assumed to be 70% [38] for the basic conditions described in this paper. The same approach can be used to calculate the cooler's effectiveness.

### 3.2 Model simulation environment and verification

#### 3.2.1 Simulation environment

The numerical model was established in the MATLAB/Simulink environment, and the parameters of the model were set according to the dimensions of the LJEG prototype from Ref. [18]. When necessary, modifications to some specific parameters are made during the follow-up parameter sensitivity analysis. In this research, a solver with a constant step size of $1\times10^{-6}$ was selected for the simulation model. Such a step size could ensure computational efficiency while maintaining a certain level of computational accuracy.

#### 3.2.2 Model validation

The open-cycle LJEG prototype developed by Newcastle University is used to assess the veracity of the developed numerical model. The rendering image and photograph of the prototype is shown in Figure 5. It has an expansion cylinder with a diameter of 80.0 mm, a compressor cylinder with a diameter of 66.0 mm, a maximum piston stroke of 120.0 mm, and a connecting rod diameter of 10.0 mm. The system's movable components have a combined mass of 8.5 kg. Detailed parameters for the open cycle LJEG prototype are provided in Table 1. During experiments, the expander’s inlet pressure was set at 2.7 bar.

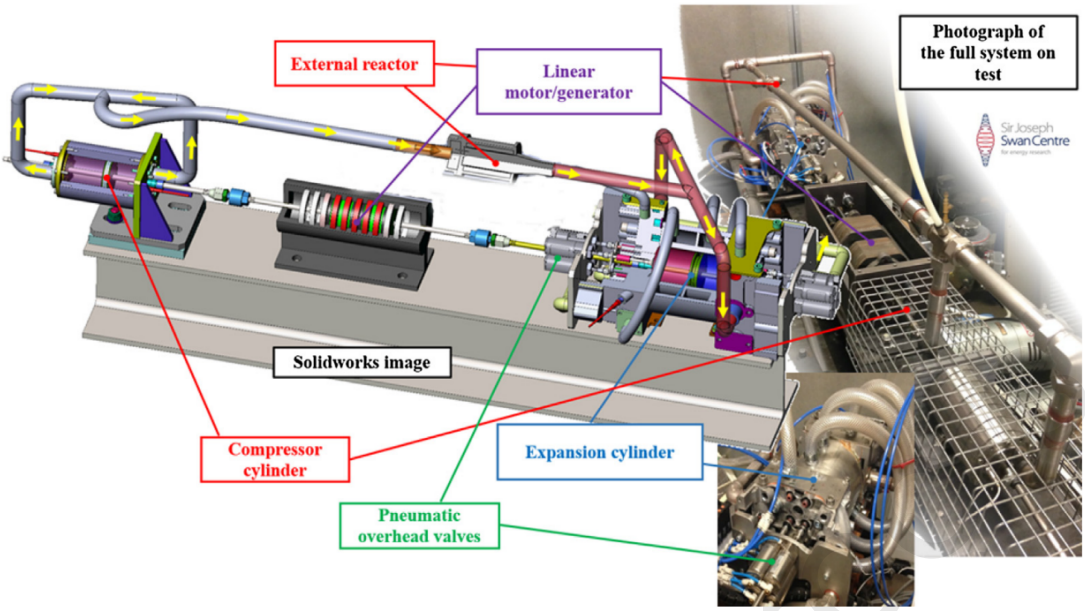


**Figure 5.** The LJEG prototype developed by members of the research team [18].

**Table 1.** The fundamental parameters of the LJEG prototype [19, 40]

| Components | Parameters [Unit] | Value |
|---|---|---|
| Expander | Moving mass [kg] | 8.5 |
| | Maximum stroke [mm] | 120.0 |
| | Cylinder diameter [mm] | 80.0 |
| | Inlet pressure [bar] | 7.0 |
| | Inlet temperature [K] | 1100.0 |
| Compressor | Maximum stroke [mm] | 120.0 |
| | Cylinder diameter [mm] | 66.0 |

| | |
|---|---|
| Inlet pressure [bar] | 1.0 |
| Outlet pressure [bar] | 7.0 |

The closed-cycle LJEG model developed above is modified to suit the open-cycle LJEG prototype and validate the accuracy of the developed numerical model. Figure 6 compares the simulation results and the experimental results (obtained from the prototype at Newcastle University) of piston velocity, piston displacement, and pressure variations in the expander and compressor cylinders profiles. The simulation results indicate that the model agrees well with the test data for piston motion, accurately reflecting the system's operating frequency and related characteristics. Although slight discrepancies are observed in the pressure fluctuations of the expander and compressor cylinders, the overall trends remain consistent, demonstrating the model's reliability within an acceptable range. These findings indicate that the model can effectively evaluate the operating characteristics of the closed-cycle LJEG.

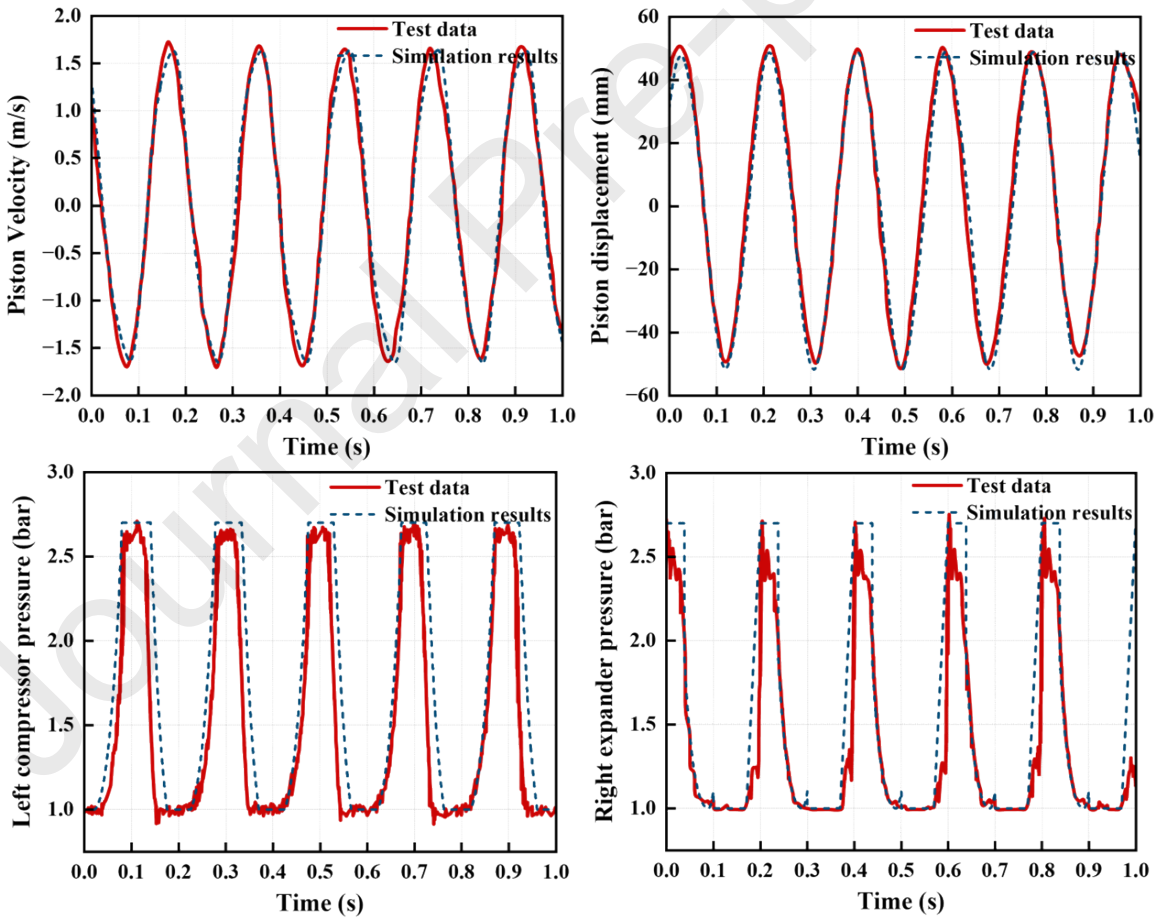


**Figure 6.** Comparison between the simulation results and the experimental results of the LJEG. The experimental results are from Ref. [40].

## 4. Results and discussions

The basic parameters of the LJEG considered in this paper are presented in Table 1. These parameters are used in Section 4 to explore the basic operating characteristics of the closed-cycle system and are also employed for comparisons with the open-cycle system. Additionally, the working fluid's entry temperature into the compressor was designated at 300 K and the discharge pressure was set to 1.1 bar to facilitate comparison with the open-cycle system. The electrical resistance coefficient of the linear generator was set to 525.69 N/(m·s$^{-1}$) by default to exclude the effects of varying electrical resistance coefficients on the system's operational efficiency during the simulation.

### 4.1 Basic system characteristics

Figure 7 displays the expander piston's displacement and velocity profiles with time of the closed-cycle LJEG, resembling those of the open-cycle LJEG with air. Following a period of stable operation, the motion waveform of the closed-cycle LJEG's piston resembles a periodic sinusoidal wave to some extent. A comprehensive comparison between the open-cycle system and the closed-cycle one will be reflected by examining the impact of system pressure on performance. For consistency, identical geometries and system pressures were maintained for both systems during the comparisons, as detailed in Table 1. Under the current system intake pressure, the operating frequency of the system is approximately 11.9 Hz, with a maximum piston displacement is 43.4 mm.

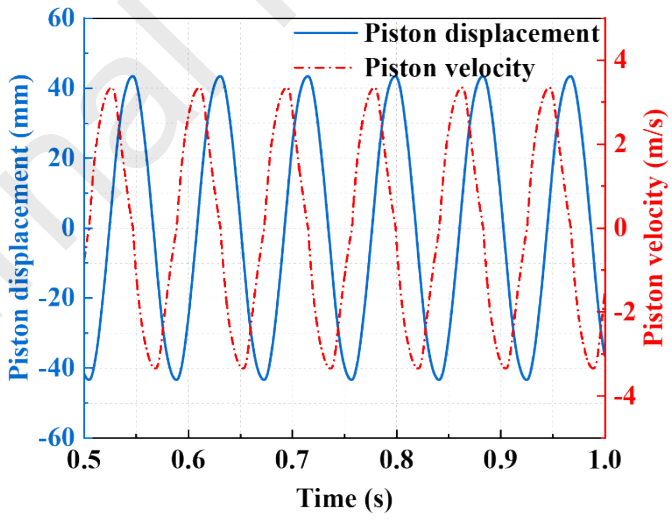


**Figure 7.** The piston's displacement and velocity profiles with time.

It was found that the timing of intake and exhaust valve openings exerts considerable influence on both system efficiency and output work. The relationship between the pressure variation within the expander cylinder and the piston position for both open-cycle and closed-cycle expanders at the same geometry and system pressure is depicted in Figure 8, with valve timing indicated. A comparison between the open-cycle air and closed-cycle helium systems

reveals a difference in the timing of the expander's intake and exhaust valve openings between the two systems. Additionally, it can be concluded from Figure 8 that the output power of the expander (the area surrounded by the pressure-displacement curve) of the closed-cycle helium system is lower than that of the open-cycle air system.

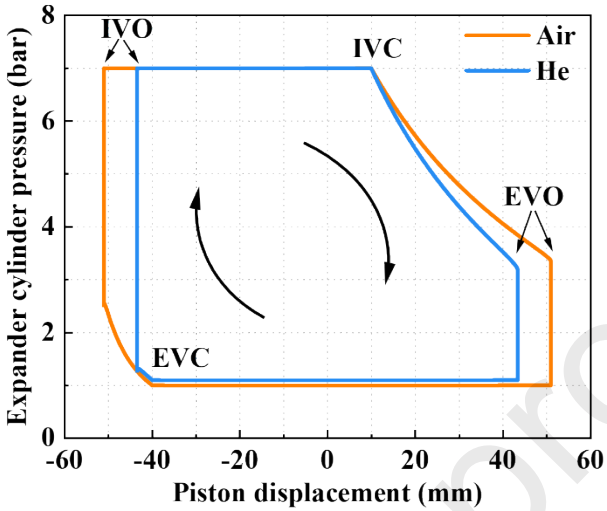


**Figure 8.** The expander cylinder pressure versus the piston displacement.

The variation of different forces acting on the mover over time of the closed-cycle system is illustrated in Figure 9. In the case of the closed-cycle system, the gas force from the expander can reach approximately 3000 N. Due to the movement of the mover and the valve timing, the peaking time of each force is different. From the above analysis, it can be observed that the gas force from the expander will push the mover to reciprocate and overcome the resistances from other components. Therefore, the setting of the expander's intake pressure significantly affects system performance. In this work, the expander intake pressure is considered the 'system pressure' for description in the following sections.

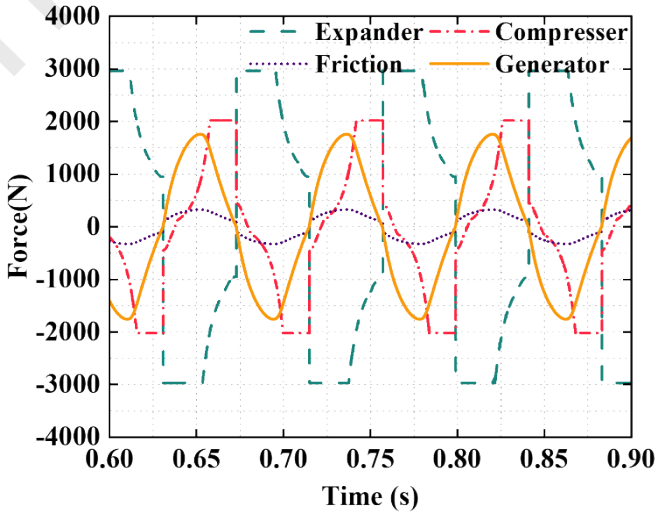


**Figure 9.** Forces versus time.

### 4.2 Effect of key parameters

This section examines the impact of key parameters, including system pressure, valve timing, electrical resistance coefficient, and cylinder diameters of the compressor and the expander is studied. This will present an insight into the impact of these parameters on the system's performance, thus offering valuable guidance for subsequent system design endeavours.

#### 4.2.1 Effect of system pressure

The system pressure plays a crucial role in determining the output power and the efficiency of the LJEG. To explore the effects of system pressure on piston dynamics and system performance, a range of pressures from 5.0 to 9.0 bar were examined for both the open-cycle system with air and the closed-cycle system with helium.

Figure 10(a) depicts the piston peak velocity for both open-cycle and closed-cycle systems at different pressures while keeping other parameters constant. Observing the figure, the greater the system pressure, the greater the peak velocity of the piston. Under different system pressures, the maximum piston stroke and operating frequency for the two systems are shown in Figures 10(b) and 10(c), respectively. With an increase of the system pressure, both the piston's amplitude and frequency increase. It is worth noting that at lower pressures, the closed-cycle helium system exhibits a higher motion frequency compared to the open-cycle air system.

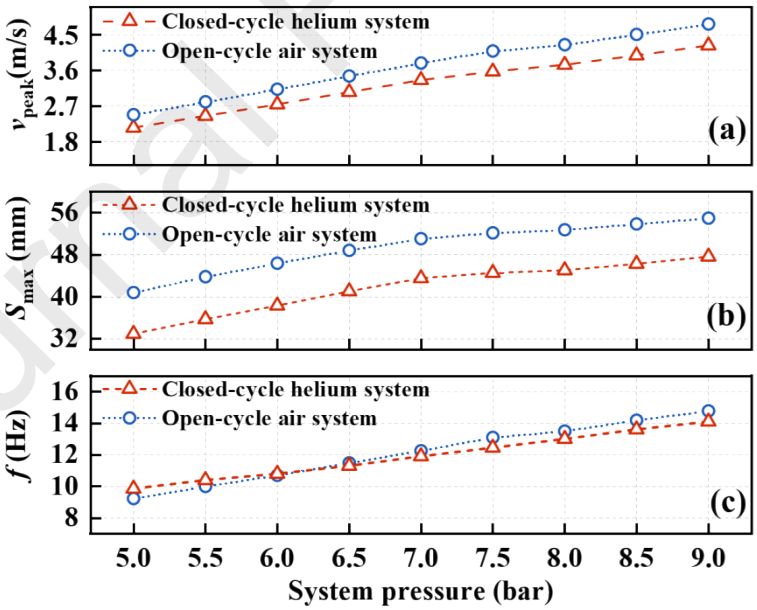


**Figure 10.** Simulation results for (a) piston velocity amplitude, (b) piston stroke amplitude, and (c) operating frequency of open-cycle air system and closed-cycle helium system at different pressures.

Figure 11 presents the output power and the efficiency of the LJEG at different system pressures. As depicted in the figure, the expander indicated power, the generator output

power, and the system efficiency increase with rising pressure. In the case of the closed-cycle helium system, as the pressure rises from 5.0 to 9.0 bar, the system's output electric power increases from 1390 to 5405 W. Although the closed-cycle system exhibits a reduction in output power compared to the open-cycle air system, its efficiency improves by approximately 40% compared to that of the open-cycle air system, primarily owing to the favourable thermodynamic properties of helium. The findings suggest that, under the condition that the system's sealing and the pressure resistance of pipes and critical components are adequately ensured, increasing the system pressure can effectively enhance its efficiency. Moreover, the adoption of working fluids with superior thermodynamic properties in closed-cycle systems further contributes to improving overall system performance.

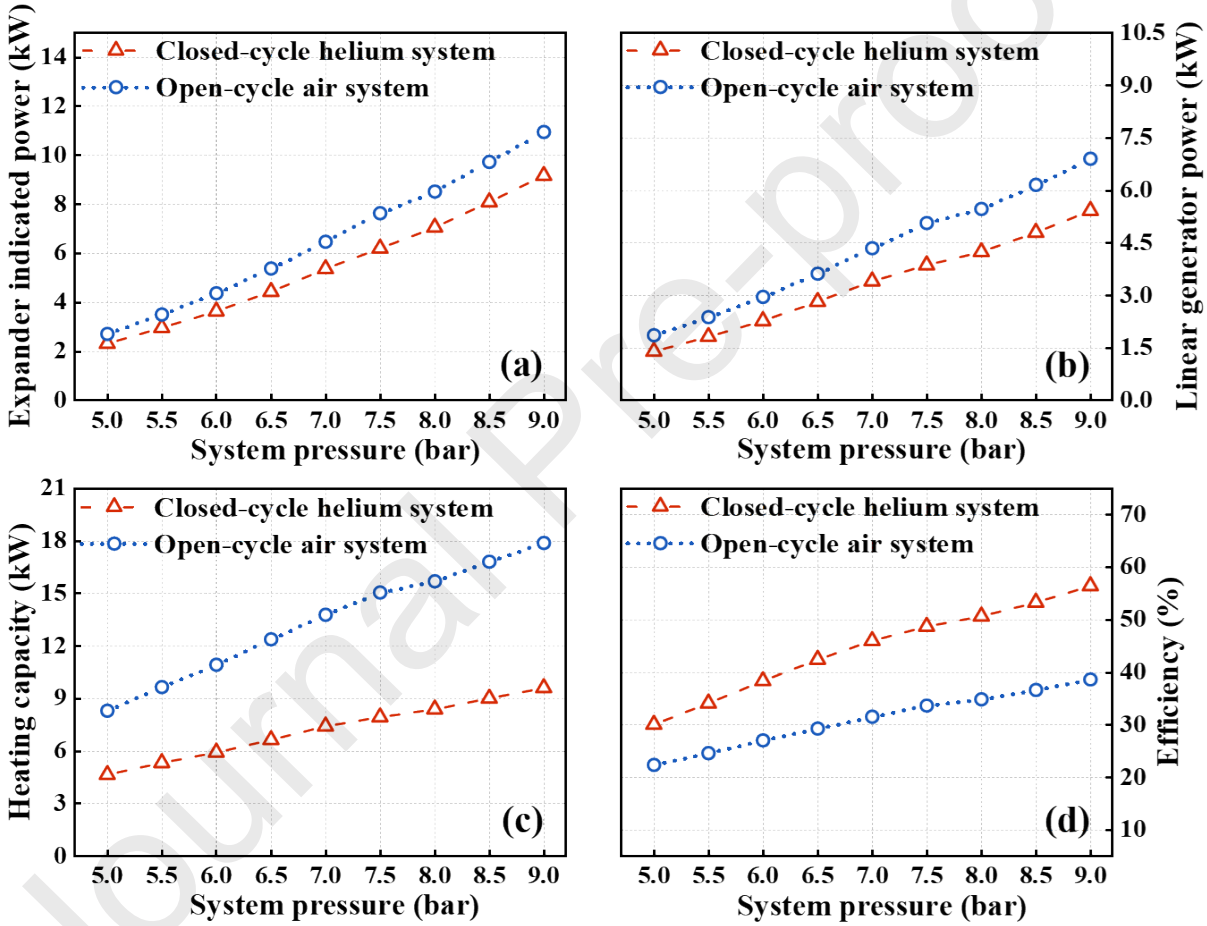


**Figure 11.** Comparisons of the (a) expander indicated power, (b) generator output power, (c) heating power, and (d) system efficiency for the closed-cycle helium system and the open-cycle air system at different pressures.

### 4.2.2 Effect of valve timing

Valve timing is a critical factor in engines, essentially not only for gasoline [41] and diesel engines [42] but also for linear Joule engines [19]. The diagram illustrating valve timing is depicted in Figure 12, with positive and negative values indicating piston positions. The intake

valve initiates opening as the expander piston arrives at its left-hand side dead centre (LDC). Subsequently, the piston moves towards the right, and the intake valve closes before the piston reaches the dead centre on the right-hand side. The distance from the piston's position when the intake valve is closed to the central stroke (the midpoint of the stroke) is referred to as the 'piston position'. A negative value for 'piston position' indicates that the intake valve closes before the central stroke, whereas a positive value indicates that it closes after the central stroke. Similarly, when the expander piston reaches its right-hand side dead centre (RDC), the exhaust valve opens. The piston then moves towards the left, and the exhaust valve closes until the piston arrives at the RDC. A negative value for 'piston position' denotes that the exhaust valve closes after the central stroke, while a positive value indicates that it closes before the central stroke.

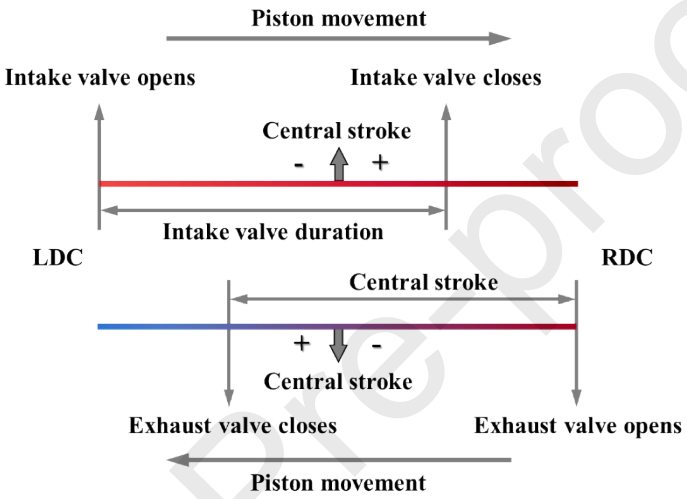


**Figure 12.** Schematic diagram of expander intake and exhaust valve timings.

To explore the impact of the expander intake valve timings on the system's operation and output performance, 9 study cases were considered under the initial condition of the system pressure being fixed at 7.0 bar as shown in Table 2. From case $A_1$ to case $A_9$, the exhaust valve opening time is fixed (it was controlled to close at 45 mm from the stroke central position), and the close timing of the intake valve was changed (see Table 2). Figure 13(a) displays the outcomes of the simulation. Notably, under the current design specifications, the heating power of the system, the expander's indicated power and the generator's output power increase with the increase in the open duration of the intake valve. As shown in Figure 13(a), with the case study number increasing, i.e., the intake valve open duration increases, the system efficiency increases and then decreases. It reaches its maximum value at case $A_6$, where the intake valve closes 15 mm from the stroke central position. In the subsequent cases $A_7$-$A_9$, an extended intake valve open duration decreased system efficiency, possibly due to the increased piston stroke and the increased friction losses.

**Table 2.** Different intake valve closing timings.

| Case number of intake valves | $A_1$ | $A_2$ | $A_3$ | $A_4$ | $A_5$ | $A_6$ | $A_7$ | $A_8$ | $A_9$ |
|---|---|---|---|---|---|---|---|---|---|

Piston position (mm) -10 -5 0 5 10 15 20 25 30

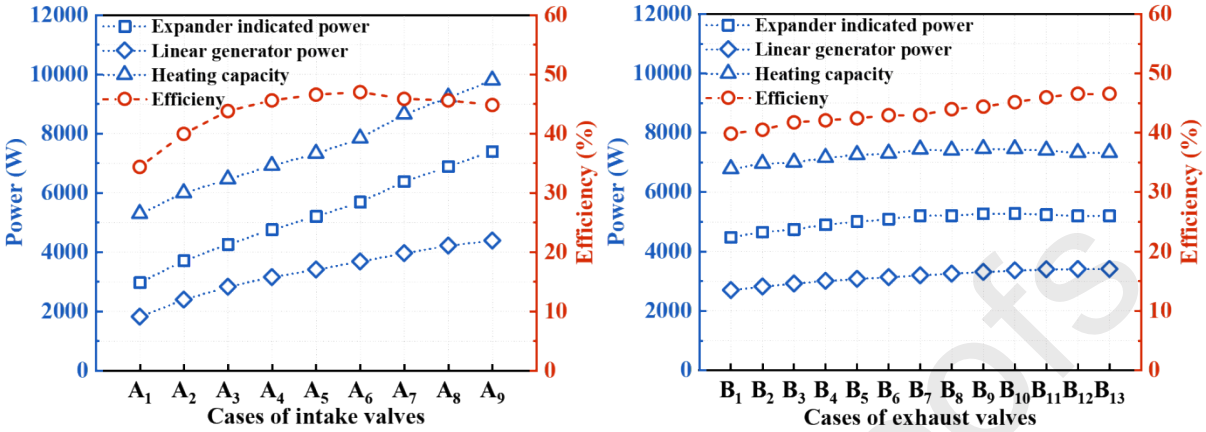


**Figure 13.** (a) System performance at different intake valve timings, and (b) system performance at different exhaust valve timings.

The impact of exhaust valve timing was studied under the condition that the intake valve was controlled to close at 10 mm, and the closing time of the exhaust valve was changed following the different exhaust valve closing timings listed in Table 3. Throughout the spectrum of case $B_1$ through case $B_{13}$, the intake valve opening time remains constant, and the exhaust valve open duration is extended accordingly. Figure 13 (b) presents the pertinent simulation outcomes. As indicated, the system's output power increases with the increase in the duration of the exhaust valve opening. The system output performance indexes in case $B_{12}$ and case $B_{13}$ are similar, indicating that when the exhaust valve close timing is set to be at a piston position of 45 mm or a piston position that is higher than 45 mm, the exhaust process is essentially adequate.

**Table 3.** Different exhaust valve closing timings.

| Case number of exhaust valves | $B_1$ | $B_2$ | $B_3$ | $B_4$ | $B_5$ | $B_6$ | $B_7$ | $B_8$ | $B_9$ | $B_{10}$ | $B_{11}$ | $B_{12}$ | $B_{13}$ |
|---|---|---|---|---|---|---|---|---|---|---|---|---|---|
| Piston position (mm) | -10 | -5 | 0 | 5 | 10 | 15 | 20 | 25 | 30 | 35 | 40 | 45 | 50 |

In summary, delaying the closing times of the intake and exhaust valves as much as possible can lead to high system output power. However, to enhance system efficiency, it is necessary to adjust the closing times of the intake and exhaust valves appropriately, especially when other operating parameters remain unchanged.

### 4.2.3 Effect of electrical resistance coefficient

The coefficient of electrical resistance determines the amount of resistance of the generator, which affects the motion state of the mover and, hence, the output performance of the LJEGs. Therefore, the simulation incorporates electrical resistance coefficients to reveal their influence on the system performance. The electrical resistance coefficients considered

are shown in Table 4, while the system pressure and valve timing are maintained as the initial settings during the simulation process. As we know, the generator load constant, $C_e$, can be expressed as:

$$C_e = \alpha C_{emax}(30)$$

where $\alpha$ represents the electrical resistance coefficient, and $C_{e\ max}$ is the maximum design value of $C_e$.

**Table 4.** Different electrical resistance coefficients.

| Case number | $C_1$ | $C_2$ | $C_3$ | $C_4$ | $C_5$ |
|---|---|---|---|---|---|
| α (-) | 0.6 | 0.7 | 0.8 | 0.9 | 1.0 |
| $C_e$(N/(m·s$^{-1}$)) | 315.41 | 367.98 | 420.55 | 473.12 | 525.69 |

Figure 14 shows the system's performance under different electrical resistance coefficients. In cases $C_2$-$C_5$, as the $\alpha$ value increases, the expander's indicated power and the generator's output power decrease. Consequently, the system's heat-to-electricity efficiency also decreases. However, in case $C_1$, when the resistance coefficient is reduced to 0.6, there is a noticeable decrease in the system's output electric power. Conversely, the whole system's efficiency still increases with the reduction of the resistance coefficient.

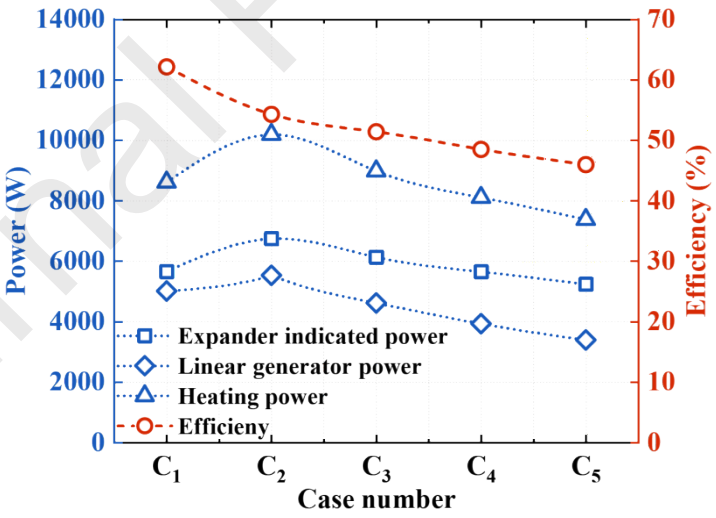


**Figure 14.** System performance under different coefficients of electrical resistance.

In case $C_1$, Figure 15 (a) illustrates the piston displacement and velocity over time. From this figure, it can be observed that under such a load condition, the movement of the piston is not symmetric about the piston's stroke central position: both the displacement and the velocity at the RDC are not symmetrically opposite to that of the LDC about the stroke central position. A further analysis of the expander piston velocity with displacement under different electrical resistance coefficients is illustrated in Figure 15 (b). Evidently, for case $C_1$, the

motion state of the expander piston is different from that of other cases. This is because the reduced coefficient of electrical resistance decreases the piston motion resistance. Therefore, the motion symmetry was affected, and asymmetric displacement and velocity profiles for case $C_1$ are observed in Figure 15 (a). With the current parameters, appropriately reducing the resistance coefficient improves the output power and system efficiency.

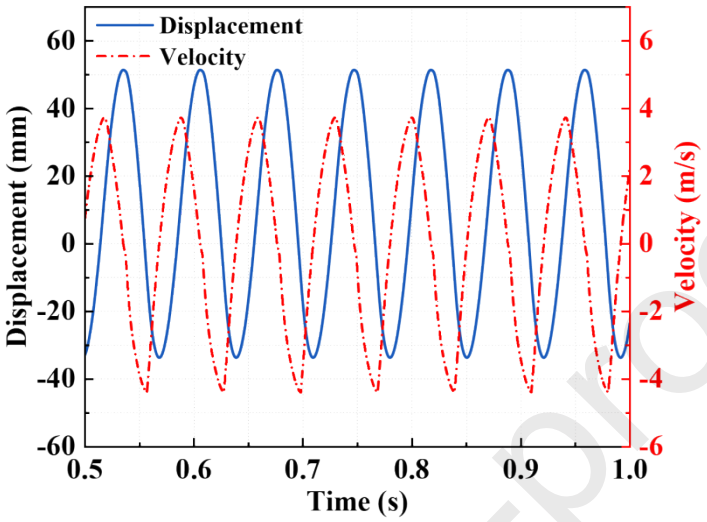


(a)

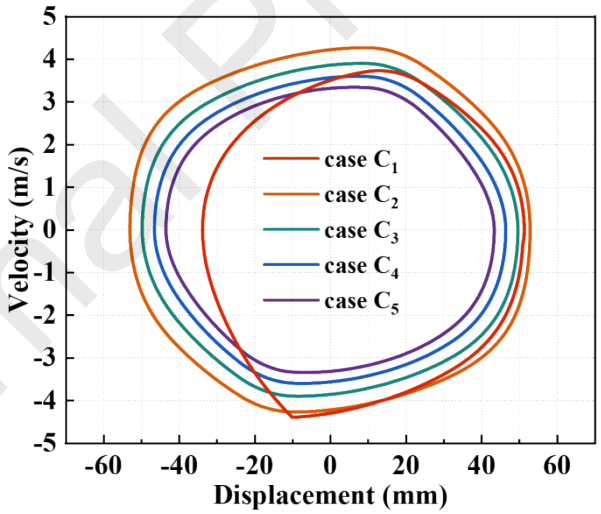


(b)

**Figure 15.** The piston's (a) displacement and (b) velocity profiles with time in case $C_1$.

### 4.2.4 Effect of cylinder diameters

For LJEG systems, the expander and compressor cylinder diameters are the most important geometric parameters. It is necessary to explore the effect of cylinder diameters of the compressor and the expander on system performance to achieve a good match between the linear Joule engine and the linear generator, thus fully exploiting the power generation

capability of the linear generator. The different diameters selected for the expander and the compressor in this study are shown in Table 5 and Table 6, respectively. Observe that when examining the influence of the compressor's cylinder diameter, the cylinder diameter of the expander is fixed at 80 mm. When examining the influence of the expander's cylinder diameter, the cylinder diameter of the compressor remains constant at 66 mm.

**Table 5.** Different compressor's cylinder diameter values.

| Case number | $D_1$ | $D_2$ | $D_3$ | $D_4$ | $D_5$ |
|---|---|---|---|---|---|
| $D_{\text{exp}}$ (mm) | 80 | 80 | 80 | 80 | 80 |
| $D_{\text{com}}$ (mm) | 80 | 73 | 66 | 59 | 52 |
| $D_{\text{exp}}/D_{\text{com}}$ | 1.00 | 1.10 | 1.21 | 1.36 | 1.54 |

**Table 6.** Different expander's cylinder diameter values.

| Case number | $E_1$ | $E_2$ | $E_3$ | $E_4$ | $E_5$ |
|---|---|---|---|---|---|
| $D_{exp}$ (mm) | 66 | 73 | 80 | 87 | 94 |
| $D_{com}$ (mm) | 66 | 66 | 66 | 66 | 66 |
| $D_{\text{exp}}/D_{\text{com}}$ | 1.00 | 1.11 | 1.21 | 1.32 | 1.42 |

Figure 16 illustrates how variations in the diameters of compressor and expander cylinders impact system performance. As seen in Figure 16(a), when the expander cylinder diameter remains constant, an increase in the compressor cylinder diameter leads to improved system efficiency. However, the linear generator's output power first increases and then decreases. As seen from Figure 16(b), within a specific range of the expander's cylinder diameter (except case $E_5$), both the output power and efficiency of the system are improved with the increase of the expansion cylinder diameter. Nevertheless, when the compressor/expander cylinder diameter ratio increases to a certain extent (as seen in the case $D_5$ and $E_5$), such as in Figure 17, the piston's motion exhibits the same asymmetric behaviour as observed when reducing the electrical resistance coefficient. Additionally, different compressor cylinder diameters will affect the mass flow rate of the working fluid, which in turn impacts the heat transfer efficiency of the heater and cooler, thereby influencing the overall system efficiency.

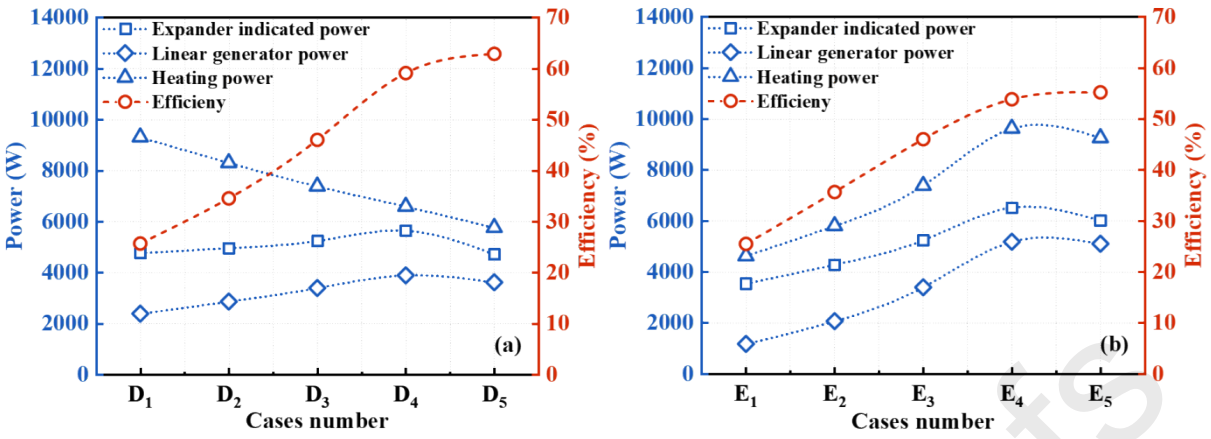


**Figure 16.** System performance under different (a) compressor cylinder diameters and (b) expander cylinder diameters.

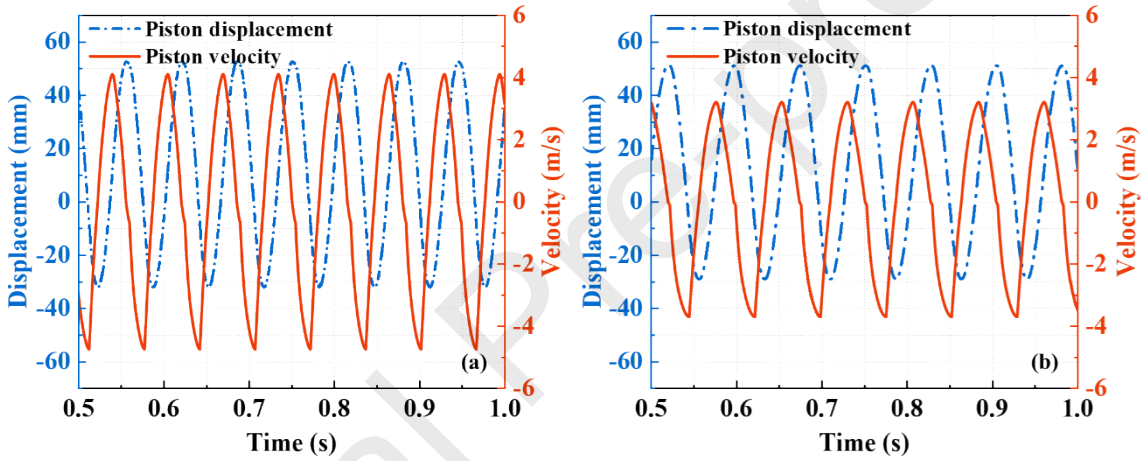


**Figure 17.** The piston motion when changing (a) the compressor diameter to the value in case $D_5$ and (b) the expander diameter to the value in case $E_5$.

## 5. Conclusions

To obtain an in-depth understanding of the operational characteristics of free-piston closed-cycle LJEGs, this paper conducts a comprehensive parameter sensitivity analysis on a free-piston closed-cycle LJEG with helium as a working fluid. Based on a validated numerical model, a comparison was made between the closed-cycle LJEG and an open-cycle LJEG under identical operating conditions. Additionally, the investigation explored the influence exerted by critical parameters such as valve timing, coefficient of electrical resistance, and cylinder diameters on system performance. The principal findings can be condensed as follows:

(1) The piston displacement and velocity profiles of the closed-cycle LJEG are analogous to those of the open-cycle LJEG. At a system pressure of 7.0 bar, the maximum

piston stroke of the closed-cycle LJEG reaches 43.4 mm, and the system operating frequency is 11.9 Hz.

(2) Within the spanned system pressure interval of 5.0 to 9.0 bar, dynamic parameters, including piston peak velocity, maximum stroke and operating frequency, and output performance indexes such as output power and efficiency, increase with system pressure in both open-cycle and closed-cycle systems. The thermodynamic properties of helium make the closed-cycle LJEG with helium more efficient than an open-cycle system with air as a working fluid, with the highest efficiency achieved in simulations exceeding 50%.

(3) In addition to system pressure, key parameters including valve timing, electrical resistance coefficient, and cylinder diameters also impact system performance. With all other parameters unchanged, the system achieves an efficiency of 46% and an electrical power of 3678 W when the expander inlet valve closes 15 mm from the stroke central position. Appropriate reduction of the electrical resistance coefficient can increase the output power and system efficiency. For the system under the geometry and working conditions set in this paper, when the electrical resistance coefficient is 367.98 $N/(m \cdot s^{-1})$, the maximum output power and efficiency can be obtained while ensuring stable operation. Expander and compressor diameters are important geometrical parameters. Under design conditions, optimal system performance is achieved and the ratio of expander diameter to compressor diameter is 1.36 (i.e., an 80 mm expander diameter and a 59 mm compressor diameter). Consequently, meticulous attention should be devoted to these parameters during the design phase of a free-piston closed-cycle LJEG.

## CRediT authorship contribution statement

**Benlei Wang**: Methodology, Investigation, Software, Formal analysis, Data Curation, Writing – original draft; **Shunmin Zhu**: Conceptualization, Funding acquisition, Validation, Supervision, Writing – review & editing; **Ugochukwu Ngwaka**: Investigation, Writing – review & editing; **Boru Jia**: Investigation, Writing – review & editing; **Kumar Vijayalakshmi Shivaprasad:** Validation, Writing – review & editing; **Yaodong Wang**: Funding acquisition, Writing – review & editing; **Andrew Smallbone**: Investigation; **Anthony Paul Roskilly**: Funding acquisition, Resources; **Ercang Luo**: Conceptualization, Supervision, Resources.

## Declaration of competing interest

The authors declare that they have no known competing financial interests or personal relationships that could have appeared to influence the work reported in this paper.

**Acknowledgments**

This research was financially supported by the European Union's Marie Skłodowska-Curie Actions Individual Fellowship (No. MSCA-IF-101026323), and the Engineering and Physical Science Research Council (EPSRC) of the United Kingdom, Impact Acceleration Account (IAA), for a project entitled, "On-board Cold Energy Recovery System For Liquid Hydrogen Fuel Cell Trucks" (No. 2273087). For the purpose of Open Access, the authors have applied a CC BY public copyright licence to any Author Accepted Manuscript version arising from this submission.

**Data Availability**

The data that support the findings of this study are available from the corresponding authors upon reasonable request.

**References**

[1] T. Zhao, H. Zhang, X. Hou, Y. Xu, J. Li, X. Shi, et al. Modelling and validation of a free piston expander-linear generator for waste heat recovery system. Appl Therm Eng. 163 (2019) 114377.

[2] Y. Chen, G. Yu, Y. Ma, J. Xue, F. Ahmed, Y. Cheng, et al. A thermally-coupled cascade free-piston Stirling engine-based cogeneration system. Appl Therm Eng. 236 (2024) 121679.

[3] R.S. Surase, R. Konijeti, R.P. Chopade. Thermally efficient gas turbine with pressure drop-based automated filter cleaning and optimized fuel control system. Appl Therm Eng. 242 (2024) 122385.

[4] H. Ghaebi, M. Yari, S.G. Gargari, H. Rostamzadeh. Thermodynamic modeling and optimization of a combined biogas steam reforming system and organic Rankine cycle for coproduction of power and hydrogen. Renewable Energy. 130 (2019) 87-102.

[5] R. Mikalsen, A.P. Roskilly. The free-piston reciprocating Joule Cycle engine: A new approach to efficient domestic CHP generation. Proceeding of ICAE2012 conference. Citeseer2012.

[6] I. Aslanidou, M. Rahman, V. Zaccaria, K.G. Kyprianidis. Micro gas turbines in the future smart energy system: fleet monitoring, diagnostics, and system level requirements. Front Mech Eng. 7 (2021) 676853.

[7] A.I. Taleb, M.A.G. Timmer, M.Y. El-Shazly, A. Samoilov, V.A. Kirillov, C.N. Markides. A single-reciprocating-piston two-phase thermofluidic prime-mover. Energy. 104 (2016) 250-65.

[8] S. Zhu, G. Yu, J. O, T. Xu, Z. Wu, W. Dai, et al. Modeling and experimental investigation of a free-piston Stirling engine-based micro-combined heat and power system. Appl Energy. 226 (2018) 522-33.

[9] S. Zhu, G. Yu, Y. Ma, Y. Cheng, Y. Wang, S. Yu, et al. A free-piston Stirling generator integrated with a parabolic trough collector for thermal-to-electric conversion of solar energy. Appl Energy. 242 (2019) 1248-58.

[10] S. Zhu, G. Yu, K. Liang, W. Dai, E. Luo. A review of Stirling-engine-based combined heat and power technology. Appl Energy. 294 (2021) 116965.

[11] P. Brosnan, G. Tian, U. Montanaro, S. Cockerill. Non-linear and multi-domain modelling of a free piston engine with linear electric machine. Energy Conversion and Management: X. 20 (2023) 100413.

[12] Y. Tian, H. Zhang, G. Li, X. Hou, F. Yu, F. Yang, et al. Experimental study on free piston linear generator (FPLG) used for waste heat recovery of vehicle engine. Appl Therm Eng. 127 (2017) 184-93.

[13] P. Brosnan, G. Tian, H. Zhang, Z. Wu, Y. Jin. Non-linear and multi-domain modelling of a permanent magnet linear synchronous machine for free piston engine generators. Energy Conversion and Management: X. 14 (2022) 100195.

[14] R. Mikalsen, A.P. Roskilly. A review of free-piston engine history and applications. Appl Therm Eng. 27 (2007) 2339-52.

[15] O. Olumayegun, M. Wang, G. Kelsall. Closed-cycle gas turbine for power generation: A state-of-the-art review. Fuel. 180 (2016) 694-717.

[16] L. Dai, Y. Sun, J. Hu, L. Zhang, Z. Wu, E. Luo. Study on the key parameters of closed-loop free-piston Brayton generator. Appl Therm Eng. 255 (2024) 124035.

[17] D. Wu, A.S. Jalal, N. Baker. A coupled model of the linear Joule engine with embedded tubular permanent magnet linear alternator. Energy Procedia. 105 (2017) 1986-91.

[18] B. Jia, D. Wu, A. Smallbone, C. Lawrence, A.P. Roskilly. Design, modelling and validation of a linear Joule Engine generator designed for renewable energy sources. Energy Convers Manage. 165 (2018) 25-34.

[19] B. Jia, D. Wu, A. Smallbone, U.C. Ngwaka, A.P. Roskilly. Dynamic and thermodynamic characteristics of a linear Joule engine generator with different operating conditions. Energy Convers Manage. 173 (2018) 375-82.

[20] M.A. Bell, T. Partridge. Thermodynamic design of a reciprocating Joule cycle engine. Proc Inst Mech Eng, Part A. 217 (2003) 239-46.

[21] R. Moss, A. Roskilly, S. Nanda. Reciprocating Joule-cycle engine for domestic CHP systems. Appl Energy. 80 (2005) 169-85.

[22] J. Wojewoda, Z. Kazimierski. Numerical model and investigations of the externally heated valve Joule engine. Energy. 35 (2010) 2099-108.

[23] U. Ngwaka, B. Jia, C. Lawrence, D. Wu, A. Smallbone, A.P. Roskilly. The characteristics of a Linear Joule Engine Generator operating on a dry friction principle. Appl Energy. 237 (2019) 49-59.

[24] D. Wu, A.P. Roskilly. Design and parametric analysis of linear Joule-cycle engine with out-of-cylinder combustion. Energy Procedia. 61 (2014) 1111-4.

[25] D. Wu, H.M. Tan, B. Jia, A.P. Roskilly. A preliminary experimental study on a lab-scale Linear Joule Engine prototype. Energy Procedia. 158 (2019) 2244-9.

[26] A.S. Jalal, N.J. Baker, D. Wu. Design of tubular Moving Magnet Linear Alternator for use with an External Combustion - Free Piston Engine. 8th IET International Conference on Power Electronics, Machines and Drives (PEMD 2016)2016. pp. 1-6.

[27] A.S. Jalal, N.J. Baker, D. Wu. The effect of power converter on the design of a Linear Alternator for use with a Joule Cycle-Free Piston Engine. 2017 IEEE International Electric Machines and Drives Conference (IEMDC)2017. pp. 1-8.

[28] A.S. Jalal, N.J. Baker, D. Wu. Electrical machine design for use in an external combustion free piston engine. 5th IET International Conference on Renewable Power Generation (RPG) 2016. IET2016. pp. 1-6.

[29] U. Ngwaka, D. Wu, J. Happian-Smith, B. Jia, A. Smallbone, C. Diyoke, et al. Parametric analysis of a semi-closed-loop linear joule engine generator using argon and oxy-hydrogen combustion. Energy. 217 (2021) 119357.

[30] M. Li, U. Ngwaka, R.M. Korbekandi, N. Baker, D. Wu, A. Tsolakis. A closed-loop linear engine generator using inert gases: A performance and exergy study. Energy. 281 (2023) 128278.

[31] G. Valenti, S. Campanari, P. Silva, N. Fergnani, A. Ravidà, G. Di Marcoberardino, et al. Modeling and Testing of a Micro-cogeneration Stirling Engine Under Diverse Conditions of the Working Fluid. Energy Procedia. 61 (2014) 484-7.

[32] Y.A. Cengel, M.A. Boles, M. Kanoğlu. Thermodynamics: an engineering approach. McGraw-hill New York2011.

[33] Z. Cheng, B. Jia, Z. Xin, H. Feng, Z. Zuo, A. Smallbone, et al. Investigation of performance of free-piston engine generator with variable-scavenging-timing technology under unsteady operation condition. Appl Therm Eng. 196 (2021) 117288.

[34] G.F. Hohenberg. Advanced approaches for heat transfer calculations. SAE Trans. (1979) 2788-806.

[35] B. Jia, Z. Zuo, G. Tian, H. Feng, A.P. Roskilly. Development and validation of a free-piston engine generator numerical model. Energy Convers Manage. 91 (2015) 333-41.

[36] J. Mao, Z. Zuo, H. Feng. Parameters coupling designation of diesel free-piston linear alternator. Appl Energy. 88 (2011) 4577-89.

[37] C.-p. Lee. Turbine-Compound Free-Piston Linear Alternator Engine. 2014.

[38] V. Zare. Role of modeling approach on the results of thermodynamic analysis: Concept presentation via thermoeconomic comparison of biomass gasification-fueled open and closed cycle gas turbines. Energy Convers Manage. 225 (2020) 113479.

[39] P.E.B. de Mello, D.B. Monteiro. Thermodynamic study of an EFGT (externally fired gas turbine) cycle with one detailed model for the ceramic heat exchanger. Energy. 45 (2012) 497-502.

[40] U.C. Ngwaka. Argon oxy-hydrogen combustion for power generation employing Linear Joule Cycle Engine Generator. Newcastle University2021.

[41] K. Yeom, J. Jang, C. Bae. Homogeneous charge compression ignition of LPG and gasoline using variable valve timing in an engine. Fuel. 86 (2007) 494-503.

[42] S. Verhelst, J. Demuynck, R. Sierens, P. Huyskens. Impact of variable valve timing on power, emissions and backfire of a bi-fuel hydrogen/gasoline engine. Int J Hydrogen Energy. 35 (2010) 4399-408.

**Declaration of interests**

☒ The authors declare that they have no known competing financial interests or personal relationships that could have appeared to influence the work reported in this paper.

☐ The authors declare the following financial interests/personal relationships which may be considered as potential competing interests:

**Highlights**

- A closed-cycle linear Joule engine generator (LJEG) using helium is considered.
- The closed-cycle LJEG was modelled and simulated using MATLAB/Simulink.
- The open-cycle and closed-cycle LJEGs were compared at different system pressures.
- The closed-cycle LJEG outperforms the open-cycle ones at the same system pressures.
- Key parameter sensitivity analysis was performed on the closed-cycle LJEG.